



Fatigue properties of AA6060-T6 butt welds made by hybrid metal extrusion & bonding

Lise Sandnes¹  | Øystein Grong^{1,2} | Torgeir Welo¹ | Filippo Berto¹ 

¹Department of Mechanical and Industrial Engineering, Norwegian University of Science and Technology (NTNU), Trondheim, Norway

²HyBond AS, NTNU Aluminium Product Innovation Center, Trondheim, Norway

Correspondence

Lise Sandnes, Department of Mechanical and Industrial Engineering, Norwegian University of Science and Technology (NTNU), Richard Birkelands vei 2b, 7491 Trondheim, Norway.
Email: lise.sandnes@ntnu.no

Abstract

The present investigation is concerned with high-cycle axial fatigue testing of a 2-mm AA6060-T6 hybrid metal extrusion & bonding (HYB) butt weld produced in the solid state using AA6082 filler metal addition. The results complement the three-point bend testing and the tensile testing done in two previous studies. In this study, optical microscope and scanning electron microscope examinations have been carried out to reveal the joint macro/microstructure and document possible surface and root defects deemed to affect fatigue life. In the as-welded condition, the HYB weld suffers from surface irregularities at the weld face and ‘kissing’ bond formation in the root region. Despite of this, the subsequent testing shows that the fatigue properties exceed those reported for comparable AA6082-T6 gas metal arc butt welds and matching those reported for corresponding high-strength laser beam and friction stir weldments.

KEYWORDS

filler metal addition, high-cycle axial fatigue testing, hybrid metal extrusion & bonding (HYB), solid state joining, thin aluminium profiles

1 | INTRODUCTION

In weldments a variety of defects and geometrical discontinuities are present, which will reduce the overall fatigue life of the component.^{1–3} In particular, aluminium fusion welds are known to be prone to fatigue failure because they suffer from gas porosity and solidification cracks.^{4–6} Moreover, they are susceptible to thermal distortions and high residual stress levels which may reduce their fatigue life.^{7,8} Friction stir (FS) welded aluminium joints, on the other hand typically demonstrate superior fatigue properties compared to conventional fusion welds.^{1,9–14} Therefore, it is widely accepted that many of the negative effects of welding in the context of engineering design are reduced using solid state joining.¹⁵ Historically, the potential for improved mechanical properties and

flexibility in handling different aluminium base metal (BM) combinations and plate thicknesses was the main motivation for the development of the FS welding (FSW) process since its early launch back in 1991. Today, this method is extensively used for a variety of joining applications within the transportation, automotive, aerospace and defence industry sectors worldwide.^{16–21}

More recently, a new, patented solid state joining method for metals and alloys has emerged, known as the hybrid metal extrusion & bonding (HYB) process.²² It is based on the principles of continuous extrusion, where the so-called PinPoint extruder is the core of the invention.^{23–25} In the HYB process, favourable features of FSW and gas metal arc welding (GMAW) are combined by allowing solid state joining through aluminium filler metal (FM) additions along with the use of an

This is an open access article under the terms of the Creative Commons Attribution License, which permits use, distribution and reproduction in any medium, provided the original work is properly cited.

© 2020 The Authors. Fatigue & Fracture of Engineering Materials & Structures published by John Wiley & Sons Ltd

appropriate groove or joint design.^{26–30} For example, in butt joining of aluminium plates and profiles using HYB, groove cross-sections up to 20 mm² can be filled with solid aluminium in one pass, ensuring metallic bonding between the FM and the BM by a combination of oxide dispersion and severe plastic deformation.^{26,27} The energy consumption of the HYB method is comparable with that of FSW when it comes to heat input and extent of heat-affected zone (HAZ) softening. This makes it particularly suitable for butt welding of thin plate products.^{27,31}

In our two previous papers, the mechanical integrity of a 2-mm AA6060-T6 HYB butt weld has been evaluated by means of bend and tensile testing.^{32,33} The three-point bend test results revealed evidence of root cracking on the retreating side (RS) of the joint along its entire length due to ‘kissing’ bond formation.³² Despite of this, the tensile properties were found to be comparable with those reported for FSW of 2-mm AA6082-T6 profiles and exceed those reported for FSW of 2-mm 6061-T6 profiles.³³

In this paper, we continue the mechanical characterisation of the same 2-mm AA6060-T6 HYB weld by performing supplementary fatigue testing. The main objective of the present work is to evaluate the fatigue properties of the HYB joint in its current developed stage, with emphasis on its macrostructural features. This will be done by conducting high-cycle axial fatigue testing of the joint, combined with optical microscopy and scanning electron microscopy (SEM) examination of the as-welded joint and broken specimens, respectively. In addition, the fatigue results will be benchmarked against literature data found for comparable thin-sheet aluminium welds produced using conventional welding techniques. It is believed that this will contribute to better understanding of the HYB joint mechanical integrity, which is crucial for further development of the process. This is the first study, ever published, on the fatigue behaviour of a HYB joint.

The remainder parts of this paper are structured as follows. First, an overview of the experimental setup and test procedures will be given. Then, the main results from the microscope examination and fatigue testing are presented, followed by a discussion of the main findings. Finally, the main conclusions of the present investigation will be given.

2 | EXPERIMENTAL

2.1 | Materials and welding conditions

The 2-mm AA6060-T6 HYB butt weld referred to above was produced in HyBond's research laboratory at the

Norwegian University of Science and Technology (NTNU). Since a full description of the pilot HYB machine at NTNU along with the experimental setup and applied welding procedure have been reported elsewhere,^{24,25,32,33} only a brief summary is given below.

Prior to welding, two 1000 mm long and 50 mm wide extruded profiles were mounted in a fixture with a 7.5 mm wide I-groove between them. In the T6 temper condition, the BM displays 0.2% offset proof (yield) strength and tensile strength values of 182 and 208 MPa, respectively.³³ During butt welding the HYB PinPoint extruder with its Ø9 mm submerged rotating pin slides along the joint line at a constant speed, filling the entire groove with solid aluminium in one pass. The FM used was a Ø1.2 mm wire of the AA6082 type produced by HyBond AS. The chemical compositions of the base and filler metals are given in Table 1, whereas Table 2 summarises the operational conditions employed in the welding trial.

2.2 | Metallographic examinations

After the butt welding operation, a single cross-sectional sample was cut from the end of the assembled profiles, as illustrated in Figure 1, and prepared for metallographic examination using standard preparation techniques. The specimen was first submerged in an alkaline solution (1-g NaOH + 100-ml H₂O) for 2–3 min. Subsequently, it was examined in an Alicona confocal optical microscope at different magnifications to reveal the macro/microstructure, and document possible surface and root defects deemed to affect the weld fatigue life.

2.3 | Axial fatigue testing

The transverse fatigue test specimens were prepared in accordance with ASTM standard E466-15.³⁴ Their locations along the joint line are highlighted in Figure 1. Two sets of fatigue specimens were prepared, both having their centre located in the weld centre, i.e. the extrusion zone (EZ). However, one set was prepared having the original extrusion thickness of 2 mm, labelled EZ, and one set having a reduced specimen thickness of 1.8 mm, labelled EZ_{red}. The latter set was made to remove the previously mentioned root defect associated with the ‘kissing’ bond formation prior to testing. Additional specimens sampling the unaffected BM were taken from a separate profile having the original thickness of 2 mm. A sketch of the fatigue specimens highlighting their dimensions is shown in Figure 2.

TABLE 1 Chemical compositions of the base and filler metals (in wt.%)

	Si	Mg	Cu	Fe	Mn	Cr	Zn	Ti	Zr	B	Other	Al
BM AA6060	0.483	0.435	-	0.176	0.038	-	0.036	0.021	-	-	0.078	Balance
FM AA6082	1.110	0.610	0.002	0.200	0.510	0.140	-	0.043	0.130	0.006	0.029	Balance

Abbreviations: BM, base metal; FM, filler metal.

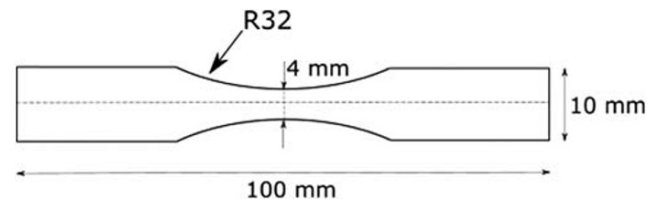
TABLE 2 Operational conditions employed in the HYB butt welding experiment with the 2-mm AA6060-T6 extruded profiles

Pin rotation (RPM)	Travel speed (mm/s)	Wire feed rate (mm/s)	Gross heat input (kJ/mm)
250	8	122	0.28

The constant-amplitude axial fatigue tests were carried out at a constant stress ratio R of 0.01 under controlled laboratory conditions at room temperature (RT). In these experiments, two different test machines were employed: an MTS Instron hydraulic test machine equipped with a load cell of 50 kN (operating at 30 Hz) and a Zwick Roell LTM10 electrodynamic test machine provided with a load cell of 10 kN (operating at 40 Hz). To obtain the desired high-cycle fatigue $S-N$ (stress–life) diagrams the maximum stress level during testing was first set to about 90% of the BM tensile strength and then gradually decreased in the subsequent tests. The fatigue life of the specimens tested was defined as the number of cycles to total failure at a given stress range. Similarly, in cases where failure did not occur the test run out was set to $2 \cdot 10^6$ cycles, in agreement with standard practice. An overview of the specimen locations, labelling and number of tests conducted along with information about the applied frequencies and machines used in the fatigue tests are given in Figure 1 and Table 3.

2.4 | Fractographic examinations

To determine the crack initiation point and the subsequent propagation direction, selected fracture surfaces of

**FIGURE 2** Schematic drawing showing the shape and dimensions of the fatigue specimens

broken fatigue specimens were examined in a Quanta FEG 450 scanning electron microscope (SEM) at different magnifications, using an acceleration voltage of 20 kV.

3 | RESULTS

3.1 | Optical microscope examinations of the weld cross-section

Figure 3 shows optical macrographs taken at different magnifications of the HYB weld cross-section. As can be seen from the low-magnification macrograph in Figure 3A, the joint appears straight and essentially free of angular distortions. However, a closer examination of the weld face in Figures 3B and 3C reveals that it is not completely smooth because of a height difference between the FM and the BM arising from a minor groove overfilling. On the advancing side (AS), the entire reinforcement edge is sharp and characterised by a total rise of about 0.15 mm. In contrast, most of the reinforcement edge on the RS is blunt, which reduces the abrupt height change at the top to 0.05 mm.

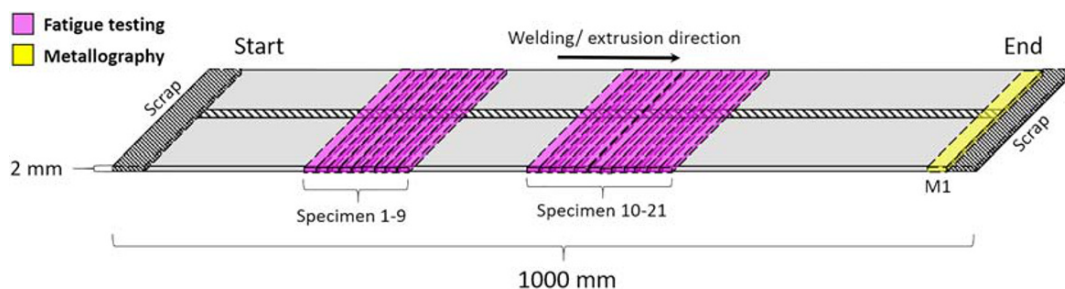
**FIGURE 1** Sketch showing the location and labelling of the different specimens used for metallographic examination (yellow) and fatigue testing (pink) referred to the start position of the weld [Colour figure can be viewed at wileyonlinelibrary.com]

TABLE 3 Summary of the applied fatigue testing conditions

Sampling area	Labelling	Thickness (mm)	Test machine	Frequency (Hz)	Total number of tests conducted
Extrusion zone	EZ	1–9	ZR ^a	40	9
	EZ _{red}	10–17	ZR	40	8
		18–21	MTS ^b	30	4
Base material	BM	22–25	ZR	40	4
		26–33	MTS	30	8

Note. Included in the table are both the location and the thickness of the specimens and their labelling along with an overview of the number of tests conducted. The specimen labelling is consistent with that used in Figure 1

^aZwick Roell LTM10 (ZR).

^bMTS Instron (MTS).

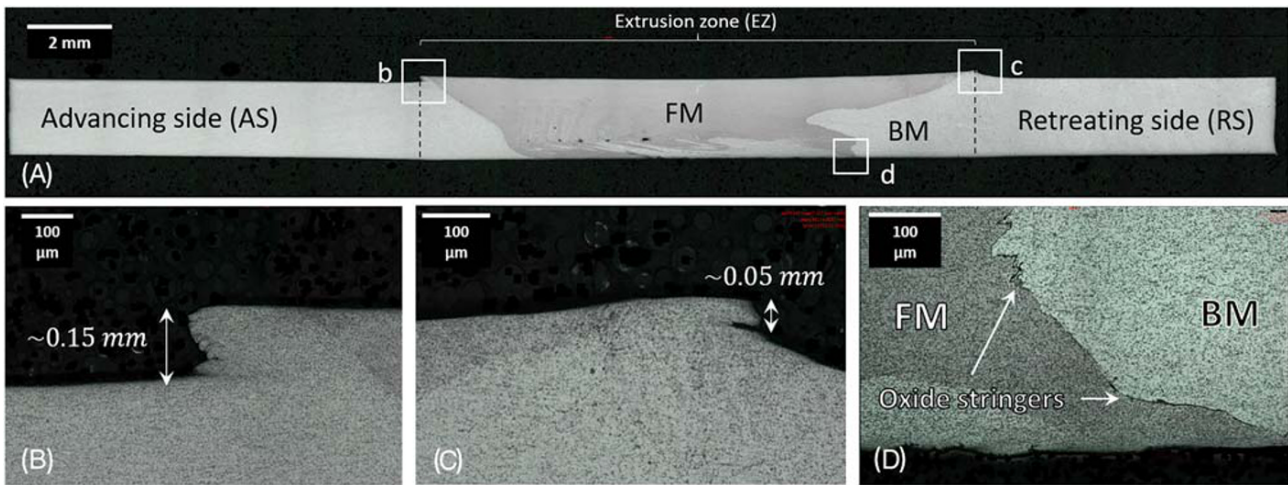


FIGURE 3 Optical macrographs of selected parts of the 2-mm HYB butt joint. (A) Picture taken at low magnification of the weld cross-section, (B) close-up of the sharp reinforcement edge observed on the AS of the joint, (C) close-up of the blunt reinforcement edge observed on the RS of the joint and (D) close-up of the FM–BM interface in the root region on the RS of the weld highlighting the embedded oxide stringers along the bond line. BM, base metal; FM, filler metal [Colour figure can be viewed at wileyonlinelibrary.com]

Moreover, Figure 3D shows a close-up of the bond line on the RS of the joint in the weld root region. This image has been included to visualise the previously mentioned ‘kissing’ bond formation, which has its origin in oxide accumulation at the FM–BM interface during welding.³²

3.2 | Fatigue properties of the BM and the EZ

The main results from the fatigue testing of the HYB joint and the BM are summarised in Figure 4. Included in the three double logarithmic S–N (stress–life) diagrams are both the measured fatigue data for specimens that failed during testing, the run-out data (denoted by a black arrow) along with a best-fit, linear regression line (i.e., the nominal or mean S–N curve) for each data set.

The mean S–N curve is given by the well-established relationship³⁵:

$$\Delta\sigma = A \cdot N_f^B, \tag{1}$$

which in the equivalent logarithmic form reads

$$\log_{10}\Delta\sigma = \log_{10}A + B\log_{10}N_f. \tag{2}$$

Note that neither the spurious data point for the BM in Figure 4A (in brackets) nor the run-out data are included in the regression analyses. Table 4 summarises the values for the constants *A* and *B* in Equation 1, the correlation coefficient *r*² and the fatigue strength at $2 \cdot 10^6$ cycles, $\Delta\sigma_{2 \cdot 10^6}$, for all three sets of test specimens.

Although the spread in the data is admittedly large, it is evident from Figure 4 and Table 4 that the BM

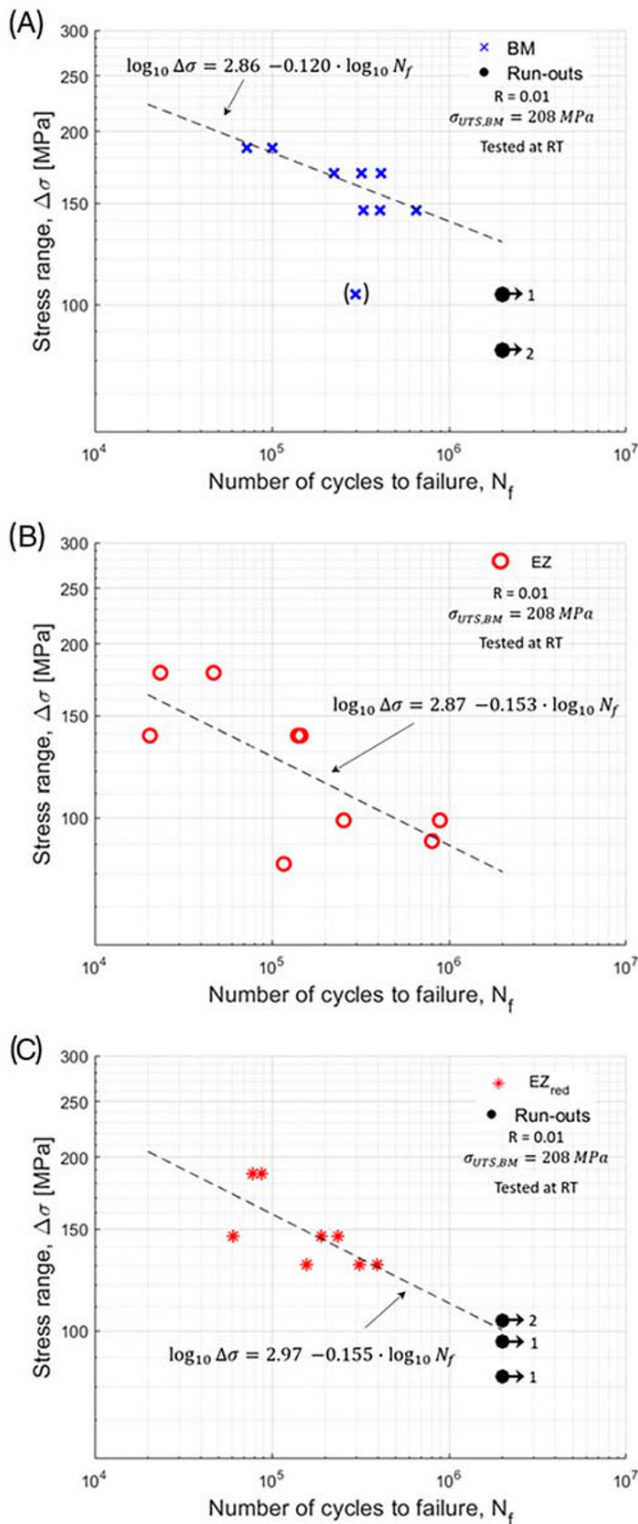


FIGURE 4 Measured fatigue data and calculated S-N curves for the base metal (BM) and the extrusion zone (EZ). (A) Specimens extracted from the BM, (B) specimens extracted from the EZ having the full thickness of 2 mm (EZ) and (C) specimens extracted from the EZ having a reduced thickness of 1.8 mm (EZ_{red}). RT, room temperature [Colour figure can be viewed at wileyonlinelibrary.com]

TABLE 4 Summary of the results from the linear regression analyses of the fatigue data presented in Figure 4

Specimen	A (MPa)	B	r^2	$\Delta\sigma_{2 \cdot 10^6}$ (MPa)
BM	729	-0.120	0.657	127
EZ	745	-0.153	0.376	81
EZ _{red}	948	-0.155	0.454	100

Note. Included in the table are the values for the constants A and B in Equation 1, the correlation coefficient r^2 and the fatigue strength at $2 \cdot 10^6$ cycles, $\Delta\sigma_{2 \cdot 10^6}$, for all three sets of test specimens. Abbreviations: BM, base metal; EZ, extrusion zone.

displays the higher fatigue properties, whereas the EZ in the as-welded condition exhibits the lower fatigue properties. The fatigue strength of the EZ_{red} specimens with reduced thickness falls in-between these two limits.

3.3 | Fracture analysis

After fatigue testing, all broken specimens were visually examined. Photographs of specimens representing EZ and EZ_{red} are shown in Figure 5. As can be seen, the location of the final fatigue failure is different in the two cases. For the EZ specimens with full thickness of 2 mm, the final fracture occurred in the weld zone at the boundary between the FM and the HAZ on the RS of the joint. In contrast, the EZ_{red} specimens with a reduced thickness of 1.8 mm failed at the boundary between the sharp FM reinforcement edge and the HAZ on the AS side of the joint.

After the visual examination, selected fracture surfaces were examined in SEM. Figure 6 shows fractographs of specimens representing the BM, EZ and EZ_{red} taken at low magnification to reveal the entire fracture surface of each individual specimen.

The results from the fractographic examination complement the previous observations in Figure 5. Whereas crack initiation in the BM specimens occurs randomly from some weak point on the surface, the fatigue crack in the EZ specimens initiates in the weld root region at the boundary between the FM and the HAZ on the RS of the joint, from which it propagates upwards towards the surface. In contrast, the fatigue crack observed in the EZ_{red} specimens initiates at the surface adjacent to the boundary between the reinforcement and the HAZ on the AS side of the joint, from which it propagates downwards towards the bottom part of the weld. These findings confirm that surface and root defects also play a major role in determining the final fatigue life of the present HYB joint.

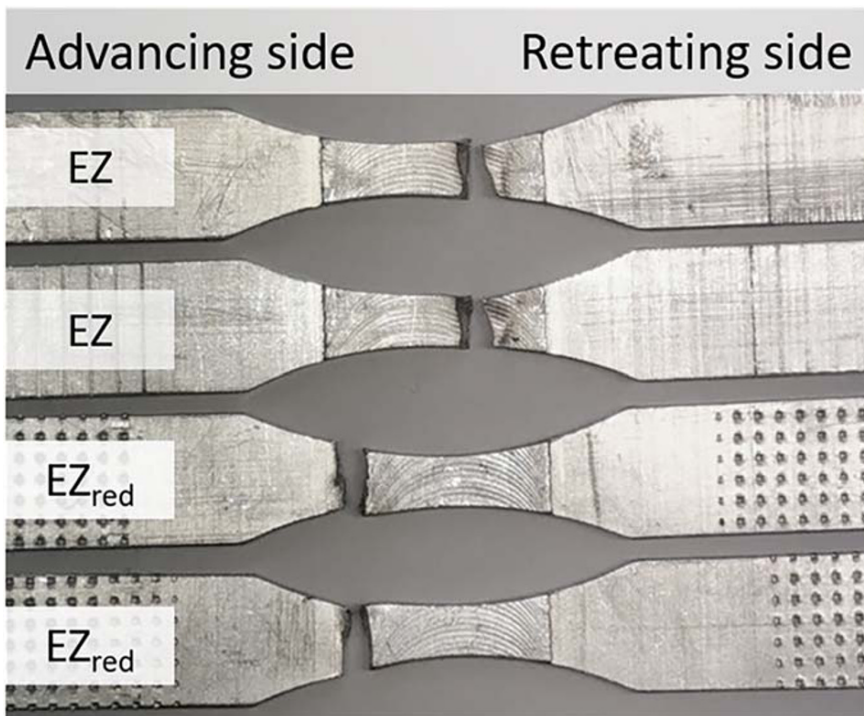


FIGURE 5 Photographs showing the location of the final fracture for selected fatigue specimens representing the EZ and the EZ_{red}. EZ, extrusion zone [Colour figure can be viewed at wileyonlinelibrary.com]

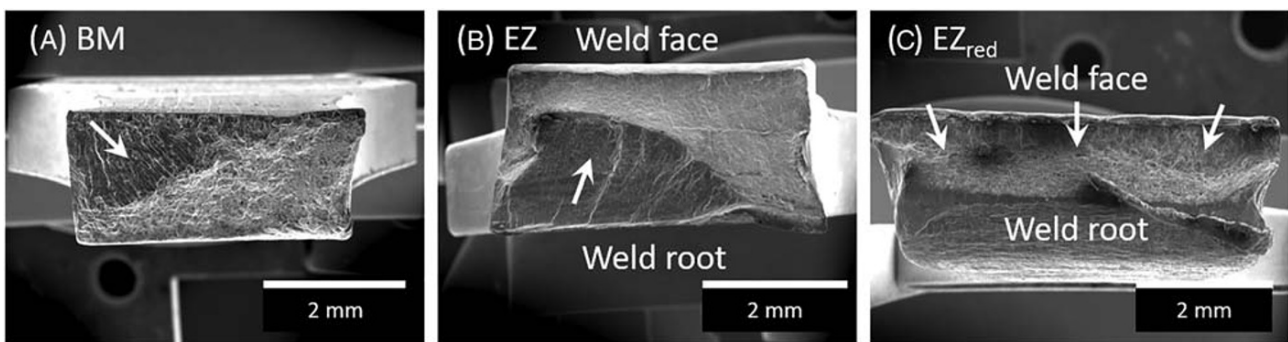


FIGURE 6 Representative scanning electron microscope fractographs of (A) the BM, (B) the EZ and (C) the EZ_{red}. The white arrows in the fractographs indicate the fatigue crack initiation point and the subsequent propagation direction. Note that all specimens are tested at a stress range of 94 MPa. BM, base metal; EZ, extrusion zone

4 | DISCUSSION

4.1 | Effects of weld defects on the fatigue strength

In welded assemblies, a variety of defects reducing the overall fatigue life of the component are present. According to Eurocode 9, the main factors affecting fatigue life of aluminium weldments are stress raisers such as geometrical discontinuities, crack-like discontinuities and tensile residual stresses, in addition to microstructural effects.³⁶ However, if actual S–N curves are available, microstructural effects are inherently accounted for.

From the optical microscope examination, it is evident that the present HYB joint suffers from both surface irregularities at the weld face and ‘kissing’ bond formation at the weld toe. Obviously, the root region on the RS of the weld is the weaker part of the joint. This is reflected by the fact that the fatigue crack in the EZ specimens with full thickness of 2 mm always initiates at the weld toe, propagating upwards towards the surface. The characteristic failure development of the 2-mm HYB butt weld is further documented by two high-magnification assembly images in Figure 7. Here, the dim fracture surface appearance of a broken EZ specimen associated with the previously mentioned ‘kissing’ bond formation can be seen.

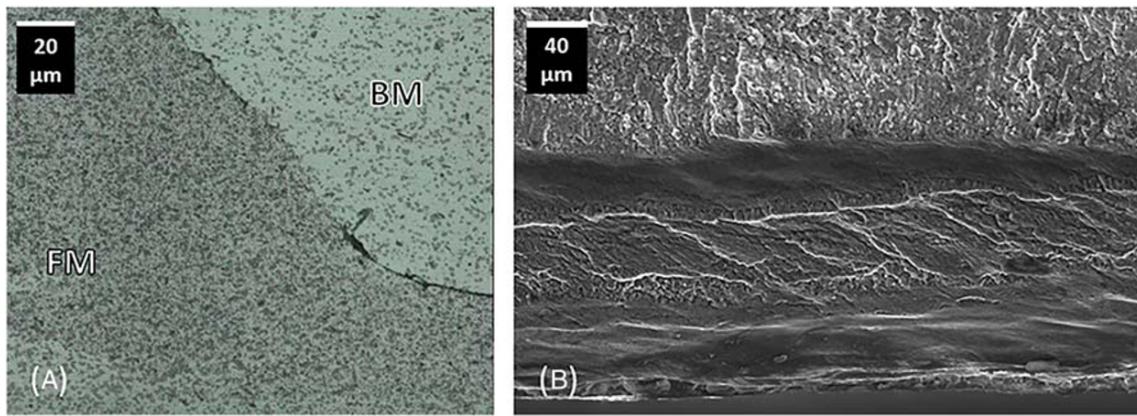


FIGURE 7 High-magnification assembly images of (A) the bond line in the root region on the retreating side of the joint and (B) the dim fracture surface appearance of a broken extrusion zone specimen associated with the ‘kissing’ bond formation in the same region. BM, base metal; FM, filler metal [Colour figure can be viewed at wileyonlinelibrary.com]

However, if the bonding defect at the weld toe is removed by machining prior to testing (as done for the EZ_{red} specimens), a change in the fatigue failure mode is observed. In that case, the fatigue crack initiates from the sharp FM reinforcement edge located at the weld face on the AS of the joint (acting as a stress raiser), from which it propagates downwards towards the bottom part of the weld through the soft HAZ. This alternative failure mode is already well documented by the images contained in Figures 5 and 6.

Note that similar observations of how weld defects affect the fatigue behaviour have also been reported for FS aluminium weldments, where the crack either initiates at surface irregularities like weld undercuts and flash ridges or at root defects.^{10,37–40} In that sense, there is no significant difference between a HYB weld and a FS weld.

4.2 | Possible effects of tensile residual stresses and weld microstructure on the fatigue strength

Figure 8 shows a comparison of the calculated S–N curves for the BM and the two sets of welded specimens, EZ and EZ_{red} . These curves have been constructed on the basis of Equation 1 and input data from Table 4, and subsequently extrapolated to fit the high-cycle fatigue domain. As can be seen from the graph, both types of welded specimens display fatigue properties that are lower than those of the BM. This is to be expected, considering the role that weld defects play in the failure development. Still, the fatigue strength of the EZ_{red} specimens does not deviate significantly from that of the BM specimens, despite the fact that the former suffers from surface irregularities at the weld face acting as stress raisers. The observed response of the EZ_{red} specimens to

fatigue testing is rather atypical for aluminium weldments. Because tensile surface residual stresses are known to have a large influence on the fatigue strength, this could indicate that the residual stress level in this particular HYB weld is low. Although quantitative measurements are not available for validation, the assumption of a low residual tensile stress level is substantiated by the fact that the 1000 mm long HYB joint in the as-welded condition appeared straight and essentially free from global distortions.³²

It is worth mentioning that other factors, such as the HYB joint microstructure and the combined use of a soft BM and a hard FM, may also contribute to the atypical response of the EZ_{red} specimens to fatigue

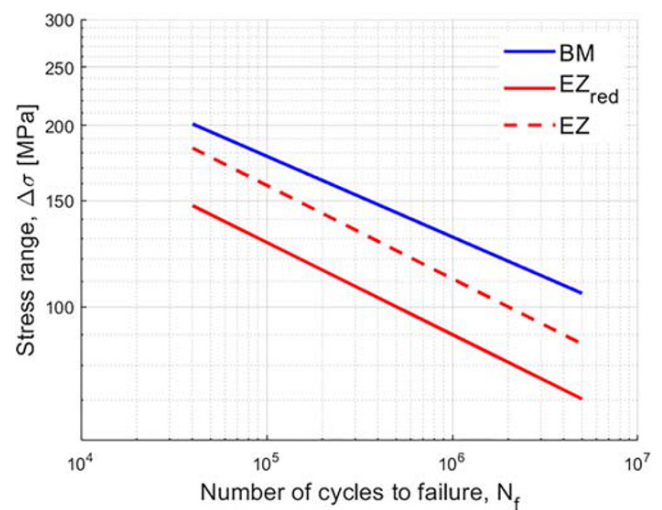


FIGURE 8 Comparison of calculated S–N curves for the BM and the different specimens sampling the EZ. Note that the curves have been constructed on the basis of Equation 1 and input data from Table 4. BM, base metal; EZ, extrusion zone [Colour figure can be viewed at wileyonlinelibrary.com]

TABLE 5 Summary of processed fatigue data for comparable Al–Mg–Si butt welds produced using GMAW, LBW and FSW

Welding process	BM	Plate thickness (mm)	UTS _{BM} (MPa)	A (MPa)	B	R-ratio	$\Delta\sigma_{2 \cdot 10^6}$ (MPa)		Source
							BM	Weld	
GMAW	6082-T6	3	323	628	−0.17	0.1	175	53	10
LBW	6061-T6	3	342	898	−0.17	0.1	175	76	10
FSW	6082-T6	3	323	523	−0.13	0.1	175	79	10

Note. Included in the table are the base metal (BM) alloy designation, plate thickness and ultimate tensile strength UTS_{BM}, the values for the constants *A* and *B* in Equation 1, the applied *R-ratio* and the fatigue strength at $2 \cdot 10^6$ cycles, $\Delta\sigma_{2 \cdot 10^6}$, for both the BM and the weld. Abbreviations: FSW, friction stir welding; GMAW, gas metal arc welding; LBW, laser beam welding.

testing. However, it is commonly believed that microstructural effects become more dominant in cases where the weld surface finish is not an issue.¹⁵ Hence, for the present combination of BM and FM, the most efficient way to bring the HYB joint fatigue properties closer to those of the BM would be to remove all surface defects through further process optimisation. To the authors' knowledge, a fatigue strength approaching that of the BM, as observed for the EZ_{red} specimens, has not yet been reported for aluminium weldments. This is, in itself, a major achievement and sets a benchmark for future testing.

4.3 | Comparison of fatigue data for different welding processes

In the following, the HYB joint fatigue properties will be benchmarked against those reported for comparable

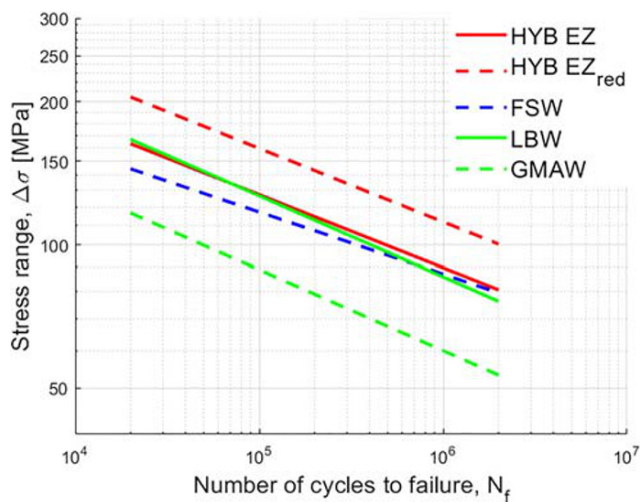


FIGURE 9 Master plot comparing linearised S–N curves for comparable Al–Mg–Si butt welds produced using different welding techniques. These curves have been constructed on the basis of Equation 1 and input data from Tables 4 and 5. EZ, extrusion zone; FSW, friction stir welding; GMAW, gas metal arc welding; HYB, hybrid metal extrusion & bonding; LBW, laser beam welding [Colour figure can be viewed at wileyonlinelibrary.com]

Al–Mg–Si butt welds produced using conventional welding techniques like GMAW, laser beam welding (LBW) and FSW.

Table 5 summarises the literature data collected for the benchmarking. They are presented in the same format as the one used for the HYB weld in Table 4 to enable a direct comparison between the different weldments. Specifically, the chosen data processing procedure involved fitting of the reported S–N curves to Equation 2 using linear regression analysis and extrapolation of the linearised curves for the fatigue strength down to $2 \cdot 10^6$ cycles, $\Delta\sigma_{2 \cdot 10^6}$. The results are presented graphically in Figure 9.

Although the applied testing conditions are not exactly the same, it is evident from Figure 9 that the fatigue properties of the 2-mm AA6060-T6 HYB butt weld exceed those reported for the 3-mm AA6082-T6 GMA butt weld, making them comparable with those reported for the corresponding high-strength LB and FS welds. Moreover, if the bonding defect at the weld toe on the RS is removed by machining prior to testing, as done for the EZ_{red} specimens, the fatigue properties of the HYB joint also exceed those of the two latter ones. This shows that the HYB process has not yet reached its ultimate potential when it comes to optimising weld fatigue strength.

5 | CONCLUSIONS

The main conclusions that can be drawn from the present study are the following.

- From the optical microscope examination, it is evident that the 2-mm AA6060-T6 HYB butt joint suffers from both surface irregularities at the weld face and 'kissing' bond formation at the weld toe.
- The as-welded HYB specimens (referred to as EZ) display lower fatigue properties compared with the base material. In the EZ specimens the fatigue crack propagates from the 'kissing bond' defect being detected at the weld toe on the RS, which is the weaker part of the joint.

- If the 'kissing bond' defect at the weld toe is removed by machining prior to testing (as done for the EZ_{red} specimens), a change in the fatigue failure mode is observed. In the EZ_{red} specimens the fatigue crack propagates from the edge in the weld reinforcement located at the weld face on the AS of the joint. Following the elimination of the 'kissing bond' defect, the fatigue strength of the HYB joint approaches that of the BM specimens, which is rather atypical for aluminium weldments. This suggests that the tensile residual stress level in the present weld is low.
- In the subsequent benchmarking of the HYB process against GMAW, LBW and FSW it is shown that the fatigue properties of the 2-mm AA6060-T6 HYB butt joint, despite the presence of bonding defects at the weld toe, exceed those of a comparable 3-mm AA6082-T6 butt weld and matches those reported for high strength LB and FS welds. However, if the bonding defect at the weld toe is removed by machining, the HYB joint fatigue properties also exceed those of the latter ones.
- From this exploratory work, it is shown that the HYB process has the potential to compete with conventional welding techniques used for thin-sheet aluminium welding when it comes to fatigue properties. However, further optimisation of the process is needed to eliminate bonding defects and surface irregularities, in order to further improve the HYB joint fatigue properties.

ACKNOWLEDGEMENTS

The authors acknowledge the financial support from HyBond AS, NTNU and NAPIC (NTNU Aluminium Product Innovation Center). They are also indebted to Luca Romere for carrying out parts of the fatigue experiments.

NOMENCLATURE

A	Constant
B	Constant
N_f	Number of cycles to failure
R	stress ratio
r^2	Correlation coefficient
$\Delta\sigma$	Stress range
σ_{UTS}	Ultimate tensile strength

ORCID

Lise Sandnes  <https://orcid.org/0000-0002-9967-4528>

Filippo Berto  <https://orcid.org/0000-0001-9676-9970>

REFERENCES

1. Maddox SJ. Review of fatigue assessment procedures for welded aluminium structures. *Int J Fatigue*. 2003;25(12):1359-1378.
2. Łagoda T, Głowacka K. Fatigue life prediction of welded joints from nominal system to fracture mechanics. *Int J Fatigue*. 2020;137:105647. <https://doi.org/10.1016/j.ijfatigue.2020.105647>
3. Fricke W. Fatigue analysis of welded joints: state of development. *Mar Struct*. 2003;16(3):185-200.
4. Grong Ø. *Metallurgical modelling of welding*. 2nd ed. Cambridge, UK: Institute of Materials; 1997.
5. Gaur V, Enoki M, Okada T, Yomogida S. A study on fatigue behavior of MIG-welded Al-Mg alloy with different filler-wire materials under mean stress. *Int J Fatigue*. 2018;107:119-129.
6. Hu YN, Wu SC, Song Z, Fu YN, Yuan QX, Zhang LL. Effect of microstructural features on the failure behavior of hybrid laser welded AA7020. *Fatigue Fract Eng Mater Struct*. 2018;41(9):2010-2023.
7. Lu Y, Zhu S, Zhao Z, Chen T, Zeng J. Numerical simulation of residual stresses in aluminum alloy welded joints. *J Manuf Processes*. 2020;50:380-393.
8. Berkovits A, Kelly D, Di S. Considerations of the effect of residual stresses on fatigue of welded aluminium alloy structures. *Fatigue Fract Eng Mater Struct*. 1998;21(2):159-170.
9. Ericsson M, Sandström R. Influence of welding speed on the fatigue of friction stir welds, and comparison with MIG and TIG. *Int J Fatigue*. 2003;25(12):1379-1387.
10. Moreira P, Richter-Trummer V, de Castro P. Fatigue behaviour of FS, LB and MIG welds of AA6061-T6 and AA6082-T6. In: *Multiscale Fatigue Crack Initiation and Propagation of Engineering Materials: Structural Integrity and Microstructural Worthiness*. Springer; 2008:85-111.
11. Texier D, Atmani F, Bocher P, et al. Fatigue performances of FSW and GMAW aluminum alloys welded joints: competition between microstructural and structural-contact-fretting crack initiation. *Int J Fatigue*. 2018;116:220-233.
12. Kim W-K, Won S-T, Goo B-C. A study on mechanical characteristics of the friction stir welded A6005-T5 extrusion. *Int J Precis Eng Manuf*. 2010;11(6):931-936.
13. Zhou C, Yang X, Luan G. Fatigue properties of friction stir welds in Al 5083 alloy. *Scr Mater*. 2005;53(10):1187-1191.
14. Maggiolini E, Benasciutti D, Susmel L, Hattingh D, James M, Tovo R. Friction stir welds in aluminium: design S-N curves from statistical analysis of literature data. *Fatigue Fract Eng Mater Struct*. 2018;41(11):2212-2230.
15. Threadgill P, Leonard A, Shercliff H, Withers P. Friction stir welding of aluminium alloys. *Int Mater Rev*. 2009;54(2):49-93.
16. Heinz A, Haszler A, Keidel C, Moldenhauer S, Benedictus R, Miller WS. Recent development in aluminium alloys for aerospace applications. *Mater Sci Eng A*. 2000;280(1):102-107.
17. Shtrikman M. Current state and development of friction stir welding part 3. Industrial application of friction stir welding. *Weld Int*. 2008;22(11):806-815.
18. Cam G, Mistikoglu S. Recent developments in friction stir welding of Al-alloys. *J Mater Eng Perform*. 2014;23(6):1936-1953.
19. Wang G-Q, Zhao Y-H, Tang Y-Y. Research Progress of bobbin tool friction stir welding of aluminum alloys: a review. *Acta Metall Sin (Engl Lett)*. 2020;33(1):13-29.
20. Deng C, Wang H, Gong B, Li X, Lei Z. Effects of microstructural heterogeneity on very high cycle fatigue properties of 7050-T7451 aluminum alloy friction stir butt welds. *Int J Fatigue*. 2016;83:100-108.

21. Cam G. Friction stir welded structural materials: beyond Al-alloys. *Int Mater Rev*. 2011;56(1):1-48.
22. Method and device for joining of metal components, particularly light metal components. United States Patent US 7131567 B2. 2006, Nov.7.
23. Grong Ø. Recent advances in solid-state joining of aluminum. *Weld J*. 2012;91(1):26-33.
24. Grong Ø, Sandnes L, Berto F. A status report on the hybrid metal extrusion & bonding (HYB) process and its applications. *Mater des Process Commun*. 2019;1(2):1-7, e41.
25. Leoni F, Grong Ø, Sandnes L, Welo T, Berto F. Finite element modelling of the filler wire feeding in the hybrid metal extrusion & bonding (HYB) process. *J Adv Joining Processes*. 2020;1:1-7.
26. Grong Ø, Sandnes L, Berto F. Progress in solid state joining of metals and alloys. *Procedia Struct Integr*. 2019;17:788-798.
27. Sandnes L, Grong Ø, Torgersen J, Welo T, Berto F. Exploring the hybrid metal extrusion and bonding process for butt welding of Al-Mg-Si alloys. *Int J Adv Manuf Technol*. 2018;98(5):1059-1065.
28. Berto F, Sandnes L, Abbatalini F, Grong Ø, Ferro P. Using the hybrid metal extrusion & bonding (HYB) process for dissimilar joining of AA6082-T6 and S355. *Procedia Struct Integr*. 2018;13:249-254.
29. Blindheim J, Grong Ø, Aakenes UR, Welo T, Steinert M. Hybrid metal extrusion & bonding (HYB)—a new technology for solid-state additive manufacturing of aluminium components. *Procedia Manuf*. 2018;26:782-789.
30. Blindheim J, Welo T, Steinert M. First demonstration of a new additive manufacturing process based on metal extrusion and solid-state bonding. *Int J Adv Manuf Technol*. 2019;105(5):2523-2530.
31. Grong Ø, Sandnes L, Bergh T, Vullum PE, Holmestad R, Berto F. An analytical framework for modelling intermetallic compound (IMC) formation and optimising bond strength in aluminium-steel welds. *Mater Des Process Commun*. 2019;1(3):1-8, e57.
32. Sandnes L, Romere L, Berto F, Welo T, Grong Ø. Assessment of the mechanical integrity of a 2 mm AA6060-T6 butt weld produced using the hybrid metal extrusion & bonding (HYB) process—part I: bend test results. *Procedia Manuf*. 2019;34:147-153.
33. Sandnes L, Romere L, Grong Ø, Berto F, Welo T. Assessment of the mechanical integrity of a 2 mm AA6060-T6 butt weld produced using the hybrid metal extrusion & bonding (HYB) process—part II: tensile test results. *Procedia Struct Integr*. 2019;17:632-642.
34. ASTM E466–15. *Standard Practice for Conducting Force Controlled Constant Amplitude Axial Fatigue Tests of Metallic Materials*. ASTM International: West Conshohocken, PA; 2015.
35. Dowling NE, Narayanasamy R, Prasad KS. *Mechanical behavior of materials: engineering methods for deformation, fracture, and fatigue*. 4th ed. Edinburgh, England: Pearson Education; 2013.
36. EN-1999. *Eurocode 9: Design of Aluminium Structures—Part 1–3: Structures Susceptible to Fatigue*. European Committee for Standardisation. 1999; 2007.
37. Aliha M, Ghoreishi S, Imani D, Fotoohi Y, Berto F. Mechanical and fracture properties of aluminium cylinders manufactured by orbital friction stir welding. *Fatigue Fract Eng Mater Struct*. 2020;43(7):1514-1528.
38. Gemme F, Verreman Y, Dubourg L, Wanjara P. Effect of welding parameters on microstructure and mechanical properties of AA7075-T6 friction stir welded joints. *Fatigue Fract Eng Mater Struct*. 2011;34(11):877-886.
39. Lomolino S, Tovo R, dos Santos J. On the fatigue behaviour and design curves of friction stir butt-welded Al alloys. *Int J Fatigue*. 2005;27(3):305-316.
40. Kashaev N, Ushmaev D, Ventzke V, Klusemann B, Fomin F. On the application of laser shock peening for retardation of surface fatigue cracks in laser beam-welded AA6056. *Fatigue Fract Eng Mater Struct*. 2020;43(7):1500-1513.

How to cite this article: Sandnes L, Grong Ø, Welo T, Berto F. Fatigue properties of AA6060-T6 butt welds made by hybrid metal extrusion & bonding. *Fatigue Fract Eng Mater Struct*. 2020; 1–10. <https://doi.org/10.1111/ffe.13302>